

A Three-loop Neutrino Mass Model with a Colored Triplet Scalar

Kingman Cheung,^{1,2,3,*} Takaaki Nomura,^{4,†} and Hiroshi Okada^{1,‡}

¹*Physics Division, National Center for Theoretical Sciences, Hsinchu, Taiwan 300*

²*Department of Physics, National Tsing Hua University, Hsinchu 300, Taiwan*

³*Division of Quantum Phases and Devices, School of Physics,
Konkuk University, Seoul 143-701, Republic of Korea*

⁴*School of Physics, KIAS, Seoul 130-722, Korea*

(Dated: May 6, 2021)

Abstract

We study a variation of the Krauss-Nasri-Trodden (KNT) model with a colored triplet scalar field and a colored singlet scalar field, in which we discuss the anomaly coming from $b \rightarrow s\mu\bar{\mu}$, fitting to the muon anomalous magnetic moment and the relic density of the Majorana-type dark matter candidate, as well as satisfying various constraints such as lepton-flavor violations and flavor-changing neutral currents. Also, we discuss the direct constraints from the collider searches and the possibilities of detecting the new fields at the LHC.

Keywords:

*Electronic address: cheung@phys.nthu.edu.tw

†Electronic address: nomura@kias.re.kr

‡Electronic address: macokada3hiroshi@cts.nthu.edu.tw

I. INTRODUCTION

The fact that neutrinos have masses perhaps is the only confirmed evidence of physics beyond the standard model (SM). Other observations which also point to physics beyond the SM, such as dark matter, dark energy, matter-antimatter asymmetry, are not as convinced as the neutrino mass. The type of models that can naturally explain the neutrino mass is based on loop diagrams, in which the smallness of neutrino mass is achieved by suppression of the loop factors. Some classic examples are the one-loop Zee model [1] and Ma model [2], two-loop Zee-Babu model [3], three-loop Krauss-Nasri-Trodden model (KNT) [4], etc.

Recently, there was a 2.6σ anomaly in lepton-universality measured in the ratio $R_K \equiv B(B \rightarrow K\mu\mu)/B(B \rightarrow Kee) = 0.745_{-0.074}^{+0.090} \pm 0.036$ by the LHCb [5]. Moreover, sizable deviations were recorded in angular distributions of $B \rightarrow K^*\mu\mu$ [6]. The results can be accounted for by a large negative contribution to the Wilson coefficient C_9 of the semileptonic operator O_9 , and also contributions to other Wilson coefficients [7].

In this work, we study a variation of the original KNT model with the original scalar fields replaced by a colored ($\bar{\mathbf{3}}$) $SU(2)_L$ -triplet field and a colored ($\mathbf{3}$) $SU(2)_L$ -singlet field (see Table II) ¹. The model can accommodate the neutrino masses and oscillation, and at the same time the model can alleviate the anomaly in $b \rightarrow s\mu\bar{\mu}$ with additional contributions to C_9 . The model also satisfies all the constraints from the lepton-flavor violations (LFV), flavor-changing neutral currents (FCNC), and the oblique parameters. Finally, we also discuss the direct constraints coming from the LHC searches and future possibilities of detecting the colored fields of the model. The most interesting channel at the LHC will be pair production of $S_{-1/3}^a S_{+1/3}^a$ followed by the decay into two jets plus missing energies.

Here we summarize the differences and improvements over the original KNT model and some other related models.

1. The original KNT model accommodates two colorless singly-charged bosons with different Z_2 charges. It always predicts one massless neutrino due to its flavor structure, but the muon $g - 2$ is always induced with a negative value [9]. On the other hand, our model has two colored leptoquark bosons with different $SU(2)_L$ charges (one is a singlet and the other is a triplet), and three massive neutrinos can be generated.

¹ Systematic analysis of this model can be found in the last entry of Table 1 in Ref. [8].

Although it potentially gives both positive and negative terms to the muon $g - 2$, the negative one unfortunately overwhelms the positive one due to the constraint from oblique parameters.

2. An alternative KNT model [11] introduced two colored leptoquark bosons, which are both $SU(2)_L$ singlets, and can then explain the neutrino oscillation data and the DM without conflicting various severe constraints arising from leptoquarks. Even though it can give positive values to the muon $g - 2$, sizable values cannot be obtained because of strong constraints from lepton-flavor violations. Also, the model does not include any sources to explain the anomaly of $B \rightarrow K^* \mu \mu$. On the other hand, our current model can explain the anomaly of $B \rightarrow K^* \mu \mu$ by modifying $C_{9(10)}$, which is the only possible way in the framework of variant KNT models. It is achieved by replacing one of the colored $SU(2)_L$ singlet boson by a colored $SU(2)_L$ triplet boson.
3. As another option, we can explain the anomaly $B \rightarrow K^* \mu \mu$ via the second class of modifications in $C'_{9(10)}$. This is achieved by introducing two colored leptoquarks in $SU(2)_L$ -doublet and hypercharges $U(1)_Y = \pm 1/6$, instead of the two leptoquarks that we mentioned in the third or fourth entry of Table 1 in Ref. [8].

This paper is organized as follows. In Sec. II, we describe the modified KNT model, the neutrino mass matrix and the solution to the anomaly in $b \rightarrow s \mu \bar{\mu}$. In Sec. III, we discuss various constraints of the model, including lepton-flavor violations, FCNC's, oblique parameters, and dark matter. In Sec. IV, we present the numerical analysis and allowed parameter space, followed by the discussion on collider phenomenology. Sec. IV is devoted for conclusions and discussion.

II. THE MODEL

In this section, we describe the model setup, derive the formulas for the active neutrino mass matrix, and calculate the contributions to $b \rightarrow s \mu \bar{\mu}$.

	Quarks			Leptons		Majorana Fermions
	$Q_{Lq_i}^a$	$u_{Rq_i}^a$	$d_{Rq_i}^a$	$L_{L\ell_i}$	$e_{R\ell_i}$	$N_{R\ell_i}$
$SU(3)_C$	3	3	3	1	1	1
$SU(2)_L$	2	1	1	2	1	1
$U(1)_Y$	$\frac{1}{6}$	$\frac{2}{3}$	$-\frac{1}{3}$	$-\frac{1}{2}$	-1	0
Z_2	+	+	+	+	+	-

TABLE I: Field contents of fermions and their charge assignments under $SU(3)_C \times SU(2)_L \times U(1)_Y \times Z_2$, where the superscript (subscript) index $a = (1, 2, 3)$ represents the color, and $q_i, \ell_i (i = 1, 2, 3)$ distinguish the generation of quarks and leptons.

	Φ	Δ^a	S^a
$SU(3)_C$	1	$\bar{3}$	3
$SU(2)_L$	2	3	1
$U(1)_Y$	$\frac{1}{2}$	$\frac{1}{3}$	$-\frac{1}{3}$
Z_2	+	+	-

TABLE II: Field contents of bosons and their charge assignments under $SU(3)_C \times SU(2)_L \times U(1)_Y \times Z_2$, where the superscript index $a = (1, 2, 3)$ represents the color.

A. Model setup

We show all the field contents and their charge assignments in Table I for the fermionic sector and Table II for the bosonic sector. Under this framework, the relevant part of the renormalizable Lagrangian and the Higgs potential are given by

$$-\mathcal{L} = (y_\ell)_{\ell_i \ell_j} \bar{L}_{L\ell_i} \Phi e_{R\ell_j} + f_{q_i \ell_j} \bar{Q}_{Lq_i}^{ca} (i\sigma_2) \Delta^a L_{L\ell_j} + g_{\ell_i q_j} \bar{N}_{R\ell_i} d_{Rq_j}^{ca} S^a + M_{N\ell_i} \bar{N}_{R\ell_i}^c N_{R\ell_i} + \text{h.c.}, \quad (\text{II.1})$$

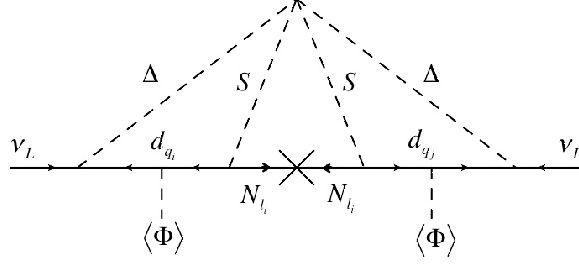


FIG. 1: The Feynman diagram for neutrino mass generation.

$$\begin{aligned}
\mathcal{V} = & m_\Phi^2 \Phi^\dagger \Phi + m_S^2 S^* S + m_\Delta^2 \text{Tr}[\Delta^{\dagger a} \Delta^a] + \lambda_0 (\text{Tr}[\Delta^a \Delta^a] S^b S^b + \text{c.c.}) \\
& + \lambda'_0 (\text{Tr}[\Delta^a \Delta^b] S^a S^b + \text{c.c.}) + \lambda''_0 (\text{Tr}[\Delta^a \Delta^b] S^a S^b + \text{c.c.}) \\
& + \lambda_\Phi |\Phi^\dagger \Phi|^2 + \lambda_S |S^{*a} S^a|^2 + \lambda_\Delta [\text{Tr}(\Delta^{\dagger a} \Delta^a)]^2 + \lambda'_\Delta \text{Tr}[(\Delta^{\dagger a} \Delta^a)]^2 + \lambda_{\Phi S} (\Phi^\dagger \Phi) (S^{*a} S^a) \\
& + \lambda_{\Phi \Delta} (\Phi^\dagger \Phi) \text{Tr}[\Delta^{\dagger a} \Delta^a] + \lambda'_{\Phi \Delta} \sum_{i=1}^3 (\Phi^\dagger \sigma_i \Phi) \text{Tr}[\Delta^{\dagger a} \sigma_i \Delta^a] + \lambda_{S \Delta} (S^{*a} S^a) \text{Tr}[\Delta^{\dagger b} \Delta^b] \\
& + \lambda'_{S \Delta} (S^{*a} S^b) \text{Tr}[\Delta^{\dagger a} \Delta^b] + \lambda''_{S \Delta} (S^{*a} S^b) \text{Tr}[\Delta^{\dagger b} \Delta^a], \tag{II.2}
\end{aligned}$$

where σ_i are the Pauli matrices, the superscript (subscript) index $a = (1, 2, 3)$ represents the color, and $q_i (i = 1, 2, 3)$ and $\ell_i (i = 1, 2, 3)$ distinguish the generation of quarks and leptons respectively. Each of λ_0 , λ'_0 , and λ''_0 comes from the contraction of $(\bar{3} \times \bar{3})(3 \times 3) \rightarrow (\bar{6}) \times (6) \rightarrow 1$, $(\bar{3} \times 3)(\bar{3} \times 3) \rightarrow (1) \times (1) \rightarrow 1$ and $(\bar{3} \times 3)(\bar{3} \times 3) \rightarrow (8) \times (8) \rightarrow 1$. Therefore, a color factor of $(6 + 1 + 8) = 15$ is multiplied to λ_0 as shown in the neutrino mass matrix, when we assume that $\lambda_0 = \lambda'_0 = \lambda''_0$.

The scalar fields can be parameterized as

$$\Phi = \begin{bmatrix} w^+ \\ \frac{v+\phi+iz}{\sqrt{2}} \end{bmatrix}, \quad \Delta = \begin{bmatrix} \frac{\delta_{1/3}}{\sqrt{2}} & \delta_{4/3} \\ \delta_{-2/3} & -\frac{\delta_{1/3}}{\sqrt{2}} \end{bmatrix}, \quad S^a \equiv S^a_{-1/3}, \tag{II.3}$$

where the subscript next to the field represents the electric charge of the field, $v = 246$ GeV, and w^\pm and z are respectively Nambu-Goldstone boson (NGB) which are absorbed by the longitudinal component of W and Z bosons. Notice that each of the components of Δ is in the mass eigenstate, since there are no mixing terms.

B. Active neutrino mass matrix

The neutrino mass matrix is induced at three-loop level as shown in Fig. 1, and its formula is given by

$$\mathcal{M}_{\nu_{ab}} \approx -\frac{60\lambda_0}{(4\pi)^6 M_{\text{Max}}^2} \sum_{i,j,k=1}^3 f_{\ell_a q_i}^T m_{d_i} g_{q_i \ell_k}^T M_{N_{\ell_k}} g_{\ell_k d_j} m_{d_j} f_{d_j \ell_b} F_3(r_{N_{\ell_k}}, r_{S_{1/3}}, r_{\delta_{1/3}}), \quad (\text{II.4})$$

$$F_3(r_{N_{\ell_k}}, r_{S_{1/3}}, r_{\delta_{1/3}}) = \int [dx] \int [dx'] \int [dx''] \times \frac{\delta(1-x-y-z)\delta(1-x'-y'-z')\delta(1-x''-y''-z'')}{x''(z'^2-z')(y'r_{S_{1/3}}+z'r_{\delta_{1/3}})+y''(z^2-z)(y'r_{S_{1/3}}+z'r_{\delta_{1/3}})-z''(z^2-z)(z'^2-z')r_{N_{\ell_k}}}, \quad (\text{II.5})$$

where $m_{d_{\{1,2,3\}}} = \{m_d, m_s, m_b\}$, $M_{\text{Max}} \equiv \text{Max}[M_{N_{\ell_k}}, m_{S_{1/3}}, m_{\delta_{1/3}}]$, $r_f \equiv m_f^2/M_{\text{Max}}^2$, $[dx] \equiv dx dy dz$, and we assume that $m_\ell \ll M_{N_{\ell_k}}, m_{S_{1/3}}, m_{\delta_{1/3}}$. Note that $F_3(r)$ is given in Ref. [9],² and $m_{S_{1/3}}$ and $m_{\delta_{1/3}}$ represent the masses of $S_{\pm 1/3}$ and $\delta_{\pm 1/3}$, respectively.

To achieve the numerical analysis of the neutrino oscillation data, we apply a method of Casas-Ibarra parametrization [10] to our neutrino mass matrix and its form is explicitly given by [11]

$$f = m_d^{-1} g^{-1} A^{-1/2} \mathcal{O} \sqrt{\mathcal{M}_\nu^{\text{diag}}} V_{MNS}^\dagger, \quad \text{or} \quad g = A^{-1/2} \mathcal{O} \sqrt{\mathcal{M}_\nu^{\text{diag}}} V_{MNS}^\dagger f^{-1} m_d^{-1}, \quad (\text{II.6})$$

where we define the diagonalization of \mathcal{M}_ν to be $\mathcal{M}_\nu^{\text{diag}} = V_{MNS}^T \mathcal{M}_\nu V_{MNS}$, and

$$A \equiv \frac{60\lambda_0 M_{N_{\ell_k}}}{(4\pi)^6 M_{\text{Max}}^2} F_3(r_{N_{\ell_k}}, r_{S_{1/3}}, r_{\delta_{1/3}}), \quad \mathcal{O} \equiv \begin{bmatrix} 1 & 0 & 0 \\ 0 & c_a & s_a \\ 0 & -s_a & c_a \end{bmatrix} \begin{bmatrix} c_b & s_b & 0 \\ -s_b & c_b & 0 \\ 0 & 0 & 1 \end{bmatrix} \begin{bmatrix} c_c & 0 & s_c \\ 0 & 1 & 0 \\ -s_c & 0 & c_c \end{bmatrix}. \quad (\text{II.7})$$

Here V_{MNS} is the Maki-Nakagawa-Sakata mixing matrix [12], \mathcal{O} is an arbitrary complex orthogonal matrix $\mathcal{O}^T \mathcal{O} = 1$, and we will adopt the best-fit values of the neutrino oscillation data from the global analysis in Ref. [13] and assume one massless neutrino with normal ordering for simplicity in the numerical analysis below.

² The typical scale of F_3 in our parameter range is 10.

C. Wilson coefficients for $b \rightarrow s\bar{\ell}\ell$ decay

Both anomalies in the lepton-universality violation measured in $R_K \equiv B(B \rightarrow K\mu\mu)/B(B \rightarrow Kee)$ and the angular distributions in $B \rightarrow K^*\mu\mu$ [6] can be accounted for by the shifts in the Wilson coefficients $C_9 = -C_{10}$. Here we discuss the effective Hamiltonian characterizing the decay process:

$$\mathcal{H}_{\text{eff}}^f = -\frac{f_{q_3\ell_i}f_{\ell_jq_2}^\dagger}{4m_{\delta_{4/3}}^2} [(\bar{s}\gamma^\mu P_L b)(\bar{\ell}_j\gamma_\mu\ell_i) - (\bar{s}\gamma^\mu P_L b)(\bar{\ell}_j\gamma_\mu\gamma_5\ell_i)]. \quad (\text{II.8})$$

Then one can write down the relevant Wilson coefficients as follows:

$$(C_9)^{\ell_i\ell_j} = -(C_{10})^{\ell_i\ell_j} = -\frac{1}{C_{\text{SM}}}\frac{f_{q_3\ell_i}f_{\ell_jq_2}^\dagger}{4m_{\delta_{4/3}}^2}, \quad C_{\text{SM}} \equiv \frac{V_{tb}V_{ts}^*G_F\alpha_{\text{em}}}{\sqrt{2}\pi}, \quad (\text{II.9})$$

where $\alpha_{\text{em}} \approx 1/137$ is the fine-structure constant, $G_F \approx 1.17 \times 10^{-5} \text{ GeV}^{-2}$ is the Fermi constant, and we focus on $i = j = 2$ ($\ell_2 = \mu$) in our case. We can then compare them to the experimentally fitted values of $C_{9,10}$ for the $\mu\mu$ component obtained in Ref. [7] as follows:

$$C_9 = -C_{10} : -0.68 \text{ (best fit value)}, \quad [-0.85, -0.50] \text{ (at } 1\sigma), \quad [-1.22, -0.18] \text{ (at } 3\sigma). \quad (\text{II.10})$$

It is worthwhile to mention the LHCb measurement of $R_K = BR(B^+ \rightarrow K^+\mu^+\mu^-)/BR(B^+ \rightarrow K^+e^+e^-) = 0.745_{-0.074}^{+0.090} \pm 0.036$, which shows a 2.6σ deviation from the SM prediction. The R_K can simply be rewritten in terms of $X^\ell = C_9^\ell - C_{10}^\ell$ ($\ell = e, \mu$), and its allowed region is found to be [14, 15]; $0.7 \leq \text{Re}[X^e - X^\mu] \leq 1.5$, where the R_K data with 1σ errors are used. This constraint can be interpreted as

$$-0.75 \lesssim C_9 \lesssim -0.35, \quad (\text{II.11})$$

where $X^e \approx 0$.

We also note that flavor violating process $B \rightarrow K^*\ell\ell'$ and $B \rightarrow \ell\ell'$ can be induced by leptoquark exchange. The branching ratios of these processes are less than experimental upper limits [16, 17] if the corresponding Wilson coefficient $C_9^{\ell\ell'}$ and $C_{10}^{\ell\ell'}$ satisfy $|C_9^{\ell\ell'}(C_{10}^{\ell\ell'})| \lesssim 1.0$ [18]. Thus experimental constraints can be satisfied while achieving the best fit value of $C_9^{\mu\mu}$. Therefore we omit further discussion of these processes.

III. VARIOUS CONSTRAINTS

A. LFVs and FCNCs at tree level

Leptoquark models usually induce LFVs and FCNCs at tree level. In our case, several processes can be induced from the term containing $f_{q_i \ell_j}$ in the Lagrangian. Their contributions to the processes can be estimated in terms of the relevant coefficients of the effective Hamiltonian as [19]

$$(\mathcal{H}_{\text{eff}})_{ijkn}^{\bar{\ell}\ell\bar{d}d} = -\frac{f_{q_k \ell_j} f_{\ell_i q_n}^\dagger}{2m_{\delta_{4/3}}^2} (\bar{\ell}_i \gamma^\mu P_L \ell_j) (\bar{d}_k \gamma_\mu P_L d_n) \equiv C_{LL}^{\bar{\ell}\ell\bar{d}d} (\bar{\ell}_i \gamma^\mu P_L \ell_j) (\bar{d}_k \gamma_\mu P_L d_n), \quad (\text{III.1})$$

$$(\mathcal{H}_{\text{eff}})_{ijkn}^{\bar{\ell}\ell\bar{u}u} = -\frac{f_{q_k \ell_j} f_{\ell_i q_n}^\dagger}{2m_{\delta_{1/3}}^2} (\bar{\ell}_i \gamma^\mu P_L \ell_j) (\bar{u}_k \gamma_\mu P_L u_n) \equiv C_{LL}^{\bar{\ell}\ell\bar{u}u} (\bar{\ell}_i \gamma^\mu P_L \ell_j) (\bar{u}_k \gamma_\mu P_L u_n), \quad (\text{III.2})$$

$$(\mathcal{H}_{\text{eff}})_{ijkn}^{\bar{\nu}\nu\bar{q}q} = -\frac{f_{q_k \ell_j} f_{\ell_i q_n}^\dagger}{2m_{\delta_{1/3}}^2} (\bar{\nu}_i \gamma^\mu P_L \nu_j) (\bar{q}_k \gamma_\mu P_L q_n) \equiv C_{LL}^{\bar{\nu}\nu\bar{q}q} (\bar{\nu}_i \gamma^\mu P_L \nu_j) (\bar{q}_k \gamma_\mu P_L q_n), \quad (\text{III.3})$$

where each of the experimental bounds is summarized in Ref. [20].

$B_{d/s} \rightarrow \mu^+ \mu^-$ measurements: Recent experiments CMS [21] and LHCb [22] reported the branching fractions of $B(B_s \rightarrow \mu^+ \mu^-)$ and $B(B_d \rightarrow \mu^+ \mu^-)$, which can place useful bounds on new physics. The bounds on the coefficients of the effective Hamiltonian in Eq. (III.1) [23] are given by

$$B(B_s \rightarrow \mu^+ \mu^-): \quad 0 \lesssim |C_{LL}^{\bar{\mu}\mu\bar{s}b}| \lesssim 5 \times 10^{-9} \text{ GeV}^{-2}, \quad (\text{III.4})$$

$$B(B_d \rightarrow \mu^+ \mu^-): \quad 1.5 \times 10^{-9} \text{ GeV}^{-2} \lesssim |C_{LL}^{\bar{\mu}\mu\bar{d}b}| \lesssim 3.9 \times 10^{-9} \text{ GeV}^{-2}. \quad (\text{III.5})$$

The other modes are also given by

$$B(B_s \rightarrow e^+ e^-): \quad |C_{LL}^{\bar{e}e\bar{s}b}| \lesssim 2.54 \times 10^{-5} \text{ GeV}^{-2}, \quad (\text{III.6})$$

$$B(B_d \rightarrow e^+ e^-): \quad |C_{LL}^{\bar{e}e\bar{d}b}| \lesssim 1.73 \times 10^{-5} \text{ GeV}^{-2}, \quad (\text{III.7})$$

$$B(B_s \rightarrow \tau^+ \tau^-): \quad |C_{LL}^{\bar{\tau}\tau\bar{s}b}| \lesssim 1.2 \times 10^{-8} \text{ GeV}^{-2}, \quad (\text{III.8})$$

$$B(B_d \rightarrow \tau^+ \tau^-): \quad |C_{LL}^{\bar{\tau}\tau\bar{d}b}| \lesssim 1.28 \times 10^{-6} \text{ GeV}^{-2}. \quad (\text{III.9})$$

B. LFVs and FCNCs at the one-loop level

LFVs at one-loop level: Some processes induced at the one-loop level could give stringent constraints. In our case, $\ell_a \rightarrow \ell_b \gamma$ processes arise from the second term in Eq. (II.1) via

one-loop diagrams, and the branching ratio is given by

$$B(\ell_a \rightarrow \ell_b \gamma) = \frac{48\pi^3 C_a \alpha_{\text{em}}}{G_{\text{F}}^2 m_{\ell_a}^2} (|(a_R)_{ab}|^2 + |(a_L)_{ab}|^2), \quad (\text{III.10})$$

where $m_{a(b)}$ is the mass for the charged-lepton eigenstate, $C_a \approx (1, 1/5)$ for $(a = \mu, \tau)$, and $a_{L(R)}$ is simply given by

$$(a_R)_{ab} \approx \sum_{i=1}^3 \frac{f_{\ell_b q_i}^\dagger f_{q_i \ell_a} m_{\ell_a}}{4(4\pi)^2} \left[\frac{1}{m_{\delta_{4/3}}^2} - \frac{1}{2m_{\delta_{1/3}}^2} \right], \quad (a_L)_{ab} \approx \sum_{i=1}^3 \frac{f_{\ell_b q_i}^\dagger f_{q_i \ell_a} m_{\ell_b}}{4(4\pi)^2} \left[\frac{1}{m_{\delta_{4/3}}^2} - \frac{1}{2m_{\delta_{1/3}}^2} \right], \quad (\text{III.11})$$

where we have taken the massless limit of the SM quarks inside the loop, because these masses should be tiny comparing to the leptoquark masses as we will discuss later. Then the current experimental upper bounds are given by [24, 25]

$$B(\mu \rightarrow e \gamma) \leq 4.2 \times 10^{-13}, \quad B(\tau \rightarrow \mu \gamma) \leq 4.4 \times 10^{-8}, \quad B(\tau \rightarrow e \gamma) \leq 3.3 \times 10^{-8}. \quad (\text{III.12})$$

Muon $g-2$: The muon anomalous magnetic moment is obtained by $\Delta a_\mu \approx -m_\mu [a_L + a_R]_{\mu\mu}$ in Eq. (III.11). Experimentally, it has been measured with a high precision, and its deviation from the SM prediction is $\Delta a_\mu = \mathcal{O}(10^{-9})$ [26].

FCNCs: The term containing $g_{\ell_i q_j}$ in Eq. (II.1) gives nonzero contributions to $b \rightarrow s \gamma$, and $K^0 - \bar{K}^0$, and $B_d^0 - \bar{B}_d^0$ mixings through the one-loop box diagrams.

$B(b \rightarrow s \gamma)$: The (partial) decay rate of $b \rightarrow s \gamma$ through the box diagram is given by

$$\Gamma(b \rightarrow s \gamma) \approx \frac{\alpha_{em} m_b^5}{442368 \pi^4} \left| \frac{g_{q_3 \ell_a}^\dagger g_{\ell_a q_2} \left[m_{S_{1/3}}^6 - 6m_{S_{1/3}}^4 M_{N_{\ell_a}}^2 + 3m_{S_{1/3}}^2 M_{N_a}^4 + 2M_{N_{\ell_a}}^6 + 126m_{S_{1/3}}^2 M_{N_{\ell_a}}^4 \ln \left(\frac{m_{S_{1/3}}}{M_{N_{\ell_a}}} \right) \right]}{(m_{S_{1/3}}^2 - M_{N_{\ell_a}}^2)^4} \right|^2, \quad (\text{III.13})$$

then the branching ratio is given by

$$B(b \rightarrow s \gamma) \approx \frac{\Gamma(b \rightarrow s \gamma)}{\Gamma_{\text{tot.}}} \lesssim 3.29 \times 10^{-4}, \quad (\text{III.14})$$

where $\Gamma_{\text{tot.}} \approx 4.02 \times 10^{-13}$ GeV is the total decay width of the bottom quark, and the value on the right-handed side is the experimental upper bound [27].

$Q - \bar{Q}$ mixing: The forms of $K^0 - \bar{K}^0$, $B_d^0 - \bar{B}_d^0$, and $D^0 - \bar{D}^0$ mixings are, respectively, given by

$$\Delta m_K \approx \frac{4}{(4\pi)^2} \sum_{i,j=1}^3 \left[g_{\ell_i q_1} g_{q_2 \ell_i}^\dagger g_{q_2 \ell_j}^\dagger g_{\ell_j q_1} F_{\text{box}}^K [N_{\ell_i}, N_{\ell_j}, S_{1/3}] \right. \\ \left. + f_{\ell_i q_1}^\dagger f_{q_2 \ell_i} f_{q_2 \ell_j} f_{\ell_j q_1}^\dagger \left(\frac{F_{\text{box}}^K [\nu_i, \nu_j, \delta_{1/3}]}{4} + F_{\text{box}}^K [\ell_i, \ell_j, \delta_{4/3}] \right) \right] \lesssim 3.48 \times 10^{-15} [\text{GeV}], \quad (\text{III.15})$$

$$\Delta m_{B_d} \approx \frac{4}{(4\pi)^2} \sum_{i,j=1}^3 \left[g_{\ell_i q_3} g_{q_1 \ell_i}^\dagger g_{q_1 \ell_j}^\dagger g_{\ell_j q_3} F_{\text{box}}^B [N_{\ell_i}, N_{\ell_j}, S_{1/3}] \right. \\ \left. + f_{\ell_i q_1}^\dagger f_{q_3 \ell_i} f_{q_3 \ell_j} f_{\ell_j q_1}^\dagger \left(\frac{F_{\text{box}}^B [\nu_i, \nu_j, \delta_{1/3}]}{4} + F_{\text{box}}^B [\ell_i, \ell_j, \delta_{4/3}] \right) \right] \lesssim 3.36 \times 10^{-13} [\text{GeV}], \quad (\text{III.16})$$

$$\Delta m_D \approx \frac{4}{(4\pi)^2} \sum_{i,j=1}^3 f_{\ell_i q_1}^\dagger f_{q_2 \ell_i} f_{q_2 \ell_j} f_{\ell_j q_1}^\dagger \left(\frac{F_{\text{box}}^D [\ell_i, \ell_j, \delta_{1/3}]}{4} + F_{\text{box}}^D [\nu_i, \nu_j, \delta_{2/3}] \right) \lesssim 6.25 \times 10^{-15} [\text{GeV}], \quad (\text{III.17})$$

$$F_{\text{box}}^Q(x, y, z) = \frac{5m_Q f_Q^2}{24} \left(\frac{m_Q}{m_q + m_{q'}} \right)^2 \int \frac{\delta(1 - a - b - c - d) da db dc dd}{am_x^2 + bm_y^2 + (c + d)m_z^2}, \quad (\text{III.18})$$

where (q, q') are respectively (d, s) for K , (b, d) for B_d , and (u, c) for D , each of the last inequalities of Eqs.(III.15, III.17) represents the upper bound on the experimental values [28], and $f_K \approx 0.156$ GeV, $f_B \approx 0.191$ GeV, $f_D \approx 0.212$ GeV, $m_K \approx 0.498$ GeV, and $m_B \approx 5.280$ GeV, and $m_D \approx 1.865$ GeV. ³

C. Oblique parameters

Since Δ is a triplet under $SU(2)_L$ gauge symmetry, we need to take into account the constraints from the oblique parameters S , T and U . Here we focus on the new physics contributions to the T and S parameter, ΔT and ΔS , and the formulas are given by

$$\Delta S = \frac{1}{9\pi} \ln \left[\frac{m_{\delta_{2/3}}^2}{m_{\delta_{4/3}}^2} \right], \quad \Delta T = \frac{16\pi}{s_{tw}^2 m_Z^2} [\Pi_{\pm}(0) - \Pi_{33}(0)], \quad (\text{III.19})$$

where $s_{tw} \approx 0.22$ is the Weinberg angle, m_Z is the Z -boson mass, and $\Pi_{\pm}(0)$, $\Pi_{33}(0)$ are given in Appendix A. The experimental bounds are given by [28]

$$(0.05 - 0.09) \leq \Delta S \leq (0.05 + 0.09), \quad (0.08 - 0.07) \leq \Delta T \leq (0.08 + 0.07). \quad (\text{III.20})$$

³ Since we assume that one of the neutrino masses to be zero with normal ordering that leads to the first column in g to be almost zero, i.e., $g_{\ell_1 q_1, \ell_1 q_2, \ell_1 q_3} \approx 0$, and so these constraints can easily be evaded.

In order to avoid these constraints, we simply take $m_{\delta_{4/3}} = m_{\delta_{2/3}} = m_{\delta_{1/3}}$ in the numerical analysis, because in such a degenerate case $\Delta S = \Delta T = 0$.

D. Dark Matter

Here we identify N_{ℓ_1} as the DM candidate [29], and denote its mass to be $M_{N_{\ell_1}} \equiv M_X$. The DM annihilation cross section is p -wave dominant and the dark matter particles annihilate into the down-type quarks, via the process $N_{\ell_1} N_{\ell_1} \rightarrow d_j \bar{d}_k$ with a $S_{1/3}$ exchange with the couplings $g_{\ell_1 q_j}$ and $g_{q_k \ell_1}^\dagger$. The relic density is simply given by

$$\Omega h^2 \approx \frac{4.28 \times 10^9 x_f^2}{12 \sqrt{g^*} M_P b_{\text{eff}}}, \quad b_{\text{eff}} \simeq \frac{|(gg^\dagger)_{\ell_1 \ell_1}|^2 M_X^2 (m_{S_{1/3}}^4 + M_X^4)}{64\pi (m_{S_{1/3}}^2 + M_X^2)^4}, \quad (\text{III.21})$$

where $g^* \approx 100$, $M_P \approx 1.22 \times 10^{19}$, $x_f \approx 25$. Note that the s -wave contribution is suppressed since it is proportional to the square of the down-type quark mass. In our numerical analysis below, we use the current experimental range for the relic density: $0.11 \leq \Omega h^2 \leq 0.13$ [30].

IV. NUMERICAL ANALYSIS

All relevant formulas have been derived in the last two sections, we are going to perform numerical analysis and search for allowed parameter space, which satisfies all the constraints that we have discussed above. We prepare *10 million* random sampling points for the relevant input parameters as follows:

$$\begin{aligned} m_{\delta_{1/3}} &\in [1.2 \times M_X, 5000] \text{GeV}, \quad m_{S_{1/3}} \in [1.2 \times M_X, 5000] \text{GeV}, \\ M_{N_{\ell_1}} (\equiv M_X) &\in [0, 3000] \text{GeV}, \quad M_{N_{\ell_2}} \in [1.2 M_X, 7500] \text{GeV}, \quad M_{N_{\ell_3}} \in [M_{N_{\ell_2}}, 10000] \text{GeV}, \\ [a, b, c] &\in (2\pi) \times [-(1+i), 1+i], \quad f' \in [-3, 0], \end{aligned} \quad (\text{IV.1})$$

where we fix $\lambda_0 = 4\pi$, $m_{\delta_{4/3}} \approx m_{\delta_{2/3}} \approx m_{\delta_{1/3}}$ and define $f_{q_i \ell_j} \equiv (\pm 1) \times 10^{f'_{q_i \ell_j}}$. Notice that $f'_{q_2 \ell_2}$ and $f'_{q_3 \ell_2}$, which are taken to be large, are directly related to the requirements of $C_{9(10)}$. The lower limit of the mass $m_{S_{1/3}}$ is taken to be $1.2 M_X$ in order to avoid the coannihilation region ($m_{S_{(1/3)}} \approx M_X$) so as to satisfy the relic density of the DM. After scanning, we find 207 parameter sets, which can accommodate the neutrino oscillation data and satisfy all the constraints.

In the left plot of Fig. 2, we show the allowed region of $m_{\delta_{1/3}}$ versus C_9 to satisfy the measured relic density of DM, where the black horizontal line represents the best fit (BF) value of $C_9 (= -0.68)$, the pale-red region $[-0.85, -0.50]$ is the one at 1σ range. Notice here that we have taken the range $C_9 \in [-0.75, -0.50]$ to satisfy R_K in Eq.(II.11). We observe that the Wilson coefficient C_9 can achieve the maximal value of -0.8 , which is in agreement with the experimentally best-fitted value of C_9 .

In the right plot of Fig. 2, we show the allowed region in the M_X - $m_{S_{1/3}}$ plane to satisfy the measured relic density of DM. It suggests that the allowed mass range for the DM is distributed to the whole range in our parameter region.

We find that lower mass bound on $\delta_{1/3}$ should be about 1.6 TeV as shown in Fig. 3, although $|f_{q_1\ell_j}| (j = 1 - 3)$ runs over all the range that we take. We discuss the possible consequence of sizable $|f_{q_1\ell_2}|$ value in collider phenomenology below. Note also that relatively large values of $f_{q_3\ell_2}$ and $f_{q_2\ell_2}$ are required in order to obtain $|C_9| \gtrsim O(0.1)$ while these bi-product coupling $f_{q_3\ell_2}f_{\ell_2q_2}^\dagger$ should be $O(10^{-2})$ for $m_{\delta_{4/3}} \sim 2$ TeV, due to the constraint of the cLFV processes such as $\mu \rightarrow e\gamma$.

Another important remark is that the muon $g - 2$ is induced at the typical value of 10^{-13} with a negative sign, which does not help to explain the experimental value of $O(+10^{-9})$. Notice here that the negative sign and the small value are due to the choice $m_{\delta_{4/3}} \approx m_{\delta_{2/3}} \approx m_{\delta_{1/3}}$, which was employed to evade the constraints of ΔS and ΔT .

One of the minimal ways to induce the positive and sizable muon $g - 2$ is to introduce another leptoquark $\Phi_{7/6}$ as an $SU(2)_L$ doublet with $U(1)_Y$ $7/6$ charge [31]. It does not violate the neutrino structure, and provides a source of muon $g - 2$ such as $\bar{Q}_L \Phi_{7/6} e_R$. Also, it gives another source of the Wilson coefficients $C_9 = C_{10}$. However it does not contribute to any other phenomenologies such as neutrino mass matrix. Thus we just mention this possibility.

A. Collider Phenomenology

Collider phenomenology mainly concerns the interactions of the $\delta_{-2/3,1/3,4/3}$ bosons and $S_{-1/3}$ boson. The interactions involving the Δ and S fields with fermions can be expanded

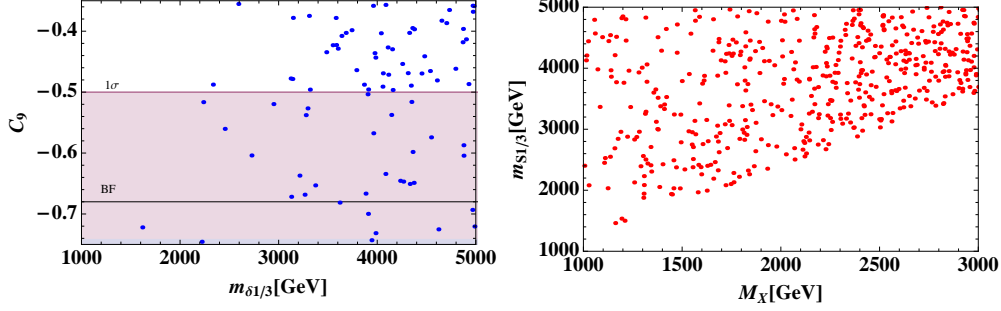


FIG. 2: Scattering plots of the allowed parameter space sets in the plane of $m_{\delta_{1/3}}-(C_9)$ in the left panel; and in the plane of $M_X-m_{S_{1/3}}$ in the right panel, where $m_{\delta_{4/3}} \approx m_{\delta_{2/3}} \approx m_{\delta_{1/3}}$ is assumed. Both points satisfy the measured relic density in $[0.11 - 0.13]$. The black horizontal line in the left panel represents the best fit (BF) value of $C_9 (= -0.68)$, the pale-red region $[-0.85, -0.50]$ is the one at 1σ range. Notice here that we have taken the range $C_9 \in [-0.75, -0.50]$ to satisfy R_K in Eq.(II.11).

as

$$\begin{aligned}
-\mathcal{L} = & f_{q_i \ell_j} \left[\overline{u_{L_i}^c} \left(\nu_{L_j} \delta_{-2/3} - \ell_{L_j} \delta_{1/3} / \sqrt{2} \right) + \overline{d_{L_i}^c} \left(-\nu_{L_j} \delta_{1/3} / \sqrt{2} - \ell_{L_j} \delta_{4/3} \right) \right] \\
& + g_{\ell_i q_j} \overline{N_{R_i}} d_{R_j}^c S_{-1/3} + h.c.
\end{aligned} \tag{IV.2}$$

The δ bosons couple to a quark and a lepton (either neutrino or charged lepton), and so they behave like leptoquarks. We first compute the decay length of the $\delta_{-2/3}$ boson: $\delta_{-2/3} \rightarrow u_{L_i}^c \bar{\nu}_{L_j}$ summing over $i, j = 1, 2, 3$. The result is

$$\Gamma(\delta_{-2/3}) = \sum_{i,j} \frac{1}{16\pi} |f_{q_i \ell_j}|^2 m_\delta. \tag{IV.3}$$

If we take $f_{q_1 \ell_2} \sim 0.1$ to be the largest among all $f_{q_i \ell_j}$ and $m_\delta = 2$ TeV, the total width of $\delta_{-2/3} \simeq 0.4$ GeV. The decay is prompt. The total widths for $\delta_{1/3}$ and $\delta_{4/3}$ are the same if their masses are the same. The current limits for prompt leptoquarks from the LHC are roughly 1 TeV, depending on the search channels [32]. Therefore, the current limits on δ bosons are also of order 1 TeV. The obvious production mode for δ bosons is then the QCD pair production [33]. The production cross section for leptoquark mass from 1 TeV to 2 TeV goes down from 10 fb to 10^{-2} fb at the LHC [33], thus rendering the pair production rather useless for the δ bosons considered here, because as shown in Fig. 3 almost all valid parameter space points have $m_\delta \gtrsim 2$ TeV. On the other hand, one may consider the single

leptoquark production is associated with a lepton, via the subprocesses, e.g., $gu \rightarrow \delta_{2/3}\bar{\nu}$, $gd \rightarrow \delta_{-4/3}\bar{\ell}$, which involve a strong coupling and a Yukawa coupling $f_{q_i\ell_j}$ in the Feynman diagram [34]. This single production may be possible to have a larger cross section than the pair production when the Yukawa coupling $f_{q_i\ell_j}$ is large enough, as there is only one heavy particle in the final state. Nevertheless, when $f_{q_i\ell_j} = e \approx 0.3$, the cross section for $m_\delta = 1$ TeV is about $O(5)$ fb while it drops down to 10^{-1} fb for $m_\delta = 2$ TeV. Since the cross section for single production is proportional to $|f_{q_i\ell_j}|^2$, it becomes 10^{-2} fb for $f_{q_i\ell_j} = 10^{-1}$. Unfortunately, the valid range of $|f_{q_1\ell_2}| \sim 0.02 - 0.2$ (See Fig. 3), such that the chance of seeing a 2 TeV δ is rather bleak.

Another way that the δ bosons can affect is the Drell-Yan production via a t -channel exchange of a δ boson, e.g., $u_{L_1}^c \bar{u}_{L_1}^c \rightarrow \ell_{L_j} \bar{\ell}_{L_{j'}}$ via $\delta_{1/3}$ or $d_{L_1}^c \bar{d}_{L_1}^c \rightarrow \ell_{L_j} \bar{\ell}_{L_{j'}}$ via $\delta_{4/3}$. Note that $|f_{12}|$ can be as large as $0.02 - 0.1$. After a Fierz transformation, the amplitude for these t -channel processes can be turned into the conventional 4-fermion contact interactions. We can then equate the coefficient of the amplitude to the contact-interaction scale as

$$\frac{|f_{q_1\ell_2}|^2}{2m_\delta^2} = \frac{4\pi}{\Lambda_{LL}^2}.$$

Using the limit $\lambda_{LL} \approx 25$ TeV quoted in PDG [28, 35], we obtain

$$m_\delta \gtrsim f_{q_1\ell_2} \times 5.0 \text{ TeV}.$$

For $|f_{q_1\ell_2}| = 0.2$ the limit on m_δ is merely 1.0 TeV. It is still less than the values shown in Fig. 3.

Now we turn to the $S_{\pm 1/3}^a$ boson, which also carries a color charge similar to a quark. It has an Z_2 -odd parity such that it has to be produced in pairs. Since it is a $SU(2)_L$ singlet with a hypercharge $-1/3$, it behaves very similar to the down-type squark \tilde{d} , \tilde{s} , or \tilde{b} . The $S_{\pm 1/3}^a$ so produced will decay into a down-type quark and a lighter right-handed neutrino $N_{R_{\ell_i}}$, which is predominantly the dark matter particle $N_{R_{\ell_1}}$. Therefore, QCD pair production of $S_{-1/3}S_{1/3}$ gives a final state of 2 jets plus missing energies. Depending on the mass difference between $S_{-1/3}$ and $N_{R_{\ell_1}}$ the jets can be very soft or energetic enough for detection: see Fig. 2. To some extent we can use the limits on the squarks if the mass difference between $S_{-1/3}$ and $N_{R_{\ell_1}}$ is large enough. For the first two generations the limits on \tilde{q} is about 1.3 TeV [36], while for the third generation the limit on sbottom is about 800 GeV [37]. Therefore, if we look back at the right panel of Fig. 2, such collider limits have no effect on the valid points. The LHC coverage at Run II can be up to about 2 – 3 TeV.

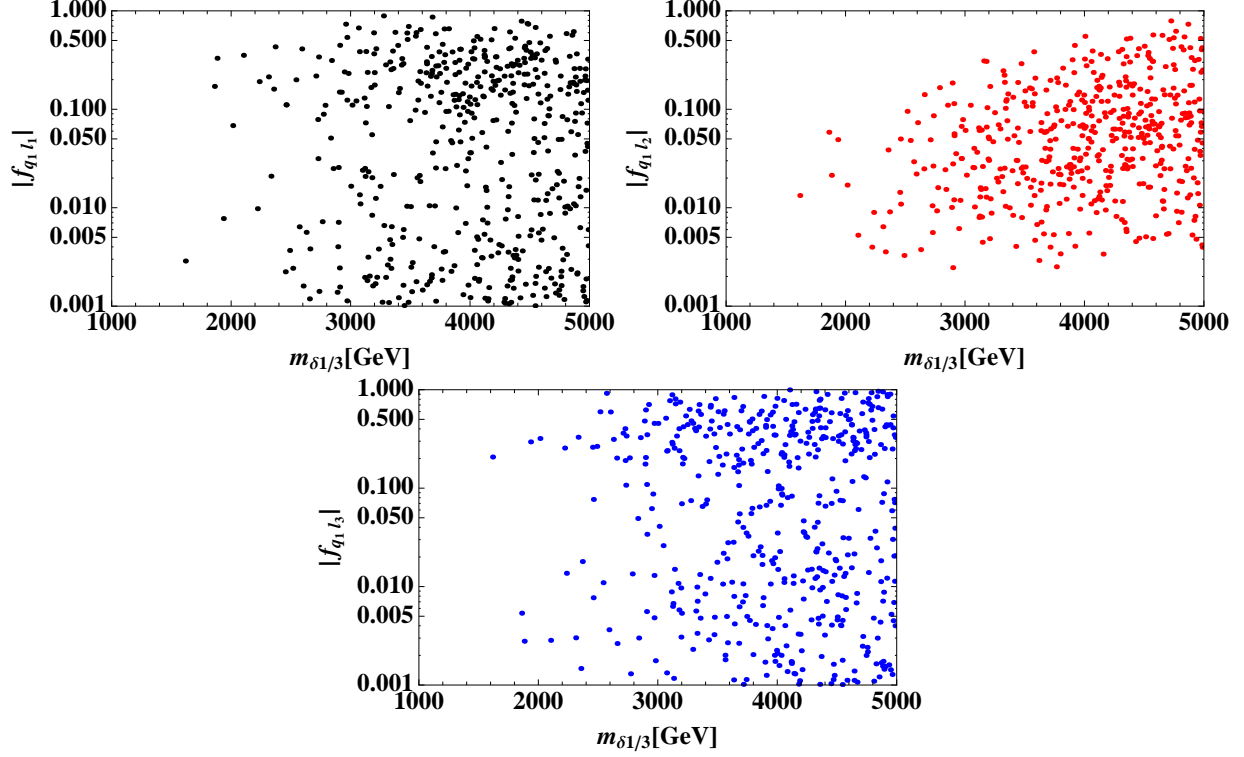


FIG. 3: Scatter plots of the allowed parameter space sets in the plane of $f_{q_1 l_j}$ versus $m_{\delta_{4/3}}$, where $m_{\delta_{4/3}} \approx m_{\delta_{2/3}} \approx m_{\delta_{1/3}}$ is assumed. The other components are almost the same as the one of $f_{q_1 l_j}$.

V. CONCLUSIONS

We have investigated a variation of the original KNT model with the scalar sector replaced by a colored $SU(2)_L$ -triplet field and a colored $SU(2)_L$ -singlet field. The model itself can afford some parameter space in accommodating all the neutrino oscillation data and satisfying all the existing LFV and FCNC constraints, as well as the relic density. We have also successfully found the parameter sets in providing solutions to the $b \rightarrow s\mu\bar{\mu}$ anomalies.

We offer a few more comments as follows.

1. The solution of the colored triplet bosons to the $b \rightarrow s\mu\bar{\mu}$ anomalies is similar to those by leptoquarks. Previous works on the anomalies and leptoquarks can be found in Ref. [38]
2. The contributions of the triplet to the muon $g - 2$ are negligible compared to the experimental uncertainties.
3. The current direct limits on the δ bosons (similar to leptoquarks) and the Drell-Yan

limits are still weaker than the lower limits that we obtain from satisfying the $b \rightarrow s\mu\bar{\mu}$ anomalies, LFV and FCNC constraints, and the DM constraint.

4. The most interesting collider signature would be the pair production of $S_{-1/3}S_{1/3}$, followed by their decays into two jets plus missing energies.

Acknowledgments

This work was supported by the Ministry of Science and Technology of Taiwan under Grants No. MOST-105-2112-M-007-028-MY3.

Appendix A: New particle contribution to vacuum polarization diagram

Here we summarize contributions to $\Pi_{\pm}(q^2)$ and $\Pi_{33}(q^2)$ in Eq. (III.19) from the new particles in our model.

Contributions to $\Pi_{\pm}(q^2)$

The one loop contributions from three-point gauge interaction are denoted by $\Pi_{\pm}^{XY}(q^2)$ where X and Y indicate particles inside loop. They are summarized as follows;

$$\Pi_{\pm}^{\delta_{1/3}\delta_{4/3}}(q^2) = \frac{2}{(4\pi)^2}G(q^2, m_{\delta_{1/3}}^2, m_{\delta_{4/3}}^2), \quad \Pi_{\pm}^{\delta_{1/3}\delta_{2/3}}(q^2) = \frac{2}{(4\pi)^2}G(q^2, m_{\delta_{1/3}}^2, m_{\delta_{2/3}}^2), \quad (\text{A.1})$$

where

$$G(q^2, m_P^2, m_Q^2) = \int dx dy \delta(1-x-y) \Delta_{PQ} [\Upsilon + 1 - \ln \Delta_{PQ}],$$

$$\Delta_{PQ} = -q^2 x(1-x) + x m_P^2 + y m_Q^2, \quad \Upsilon = \frac{2}{\epsilon} - \gamma - \ln(4\pi). \quad (\text{A.2})$$

The one loop contributions from four-point gauge interaction are denoted by $\Pi_{\pm}^X(q^2)$ where X indicates a particle inside loop. They are summarized as follows;

$$\Pi_{\pm}^{\delta_{1/3}}(q^2) = -\frac{2}{(4\pi)^2}H(m_{\delta_{1/3}}^2), \quad \Pi_{\pm}^{\delta_{2(4)/3}}(q^2) = -\frac{1}{(4\pi)^2}H(m_{\delta_{2(4)/3}}^2), \quad (\text{A.3})$$

where

$$H(m_P^2) = m_P^2 [\Upsilon + 1 - \ln m_P^2]. \quad (\text{A.4})$$

Contribution to $\Pi_{33}(q^2)$

The one loop contributions from three-point gauge interaction are denoted by $\Pi_{33}^{XY}(q^2)$ where

X and Y indicate particles inside loop. They are summarized as follows;

$$\Pi_{33}^{\delta_{2/3}\delta_{2/3}} = \frac{2}{(4\pi)^2}G(q^2, m_{\delta_{2/3}}^2, m_{\delta_{2/3}}^2), \quad \Pi_{33}^{\delta_{4/3}\delta_{4/3}} = \frac{2}{(4\pi)^2}G(q^2, m_{\delta_{4/3}}^2, m_{\delta_{4/3}}^2). \quad (\text{A.5})$$

The one loop contributions from four-point gauge interaction are denoted by $\Pi_{33,3Q,QQ}^X(q^2)$ where X indicates a particle inside loop. They are summarized as follows;

$$\Pi_{33}^{\delta_{1/3}} = -\frac{2}{(4\pi)^2}H(m_{\delta_{1/3}}^2), \quad \Pi_{33}^{\delta_{4/3}} = -\frac{2}{(4\pi)^2}H(m_{\delta_{4/3}}^2). \quad (\text{A.6})$$

-
- [1] A. Zee, Phys. Lett. B **93**, 389 (1980) Erratum: [Phys. Lett. B **95**, 461 (1980)].
doi:10.1016/0370-2693(80)90349-4, 10.1016/0370-2693(80)90193-8
- [2] E. Ma, Phys. Rev. D **73**, 077301 (2006) doi:10.1103/PhysRevD.73.077301 [hep-ph/0601225].
- [3] A. Zee, Nucl. Phys. B **264**, 99 (1986), K. S. Babu, Phys. Lett. B **203**, 132 (1988).
- [4] L. M. Krauss, S. Nasri and M. Trodden, Phys. Rev. D **67**, 085002 (2003)
doi:10.1103/PhysRevD.67.085002 [hep-ph/0210389].
- [5] R. Aaij *et al.* [LHCb Collaboration], Phys. Rev. Lett. **113**, 151601 (2014) [arXiv:1406.6482 [hep-ex]].
- [6] R. Aaij *et al.* [LHCb Collaboration], Phys. Rev. Lett. **111**, 191801 (2013) [arXiv:1308.1707 [hep-ex]].
- [7] S. Descotes-Genon, L. Hofer, J. Matias and J. Virto, JHEP **1606**, 092 (2016) [arXiv:1510.04239 [hep-ph]].
- [8] C. S. Chen, K. L. McDonald and S. Nasri, Phys. Lett. B **734**, 388 (2014)
doi:10.1016/j.physletb.2014.05.082 [arXiv:1404.6033 [hep-ph]].
- [9] K. Cheung, H. Ishida and H. Okada, arXiv:1609.06231 [hep-ph].
- [10] J. A. Casas and A. Ibarra, Nucl. Phys. B **618**, 171 (2001) [hep-ph/0103065].
- [11] T. Nomura, H. Okada and N. Okada, arXiv:1608.02694 [hep-ph].
- [12] Z. Maki, M. Nakagawa and S. Sakata, Prog. Theor. Phys. **28**, 870 (1962).
- [13] D. V. Forero, M. Tortola and J. W. F. Valle, Phys. Rev. D **90**, no. 9, 093006 (2014)
[arXiv:1405.7540 [hep-ph]].
- [14] G. Hiller and F. Kruger, Phys. Rev. D **69**, 074020 (2004) doi:10.1103/PhysRevD.69.074020 [hep-ph/0310219].

- [15] G. Hiller and M. Schmaltz, Phys. Rev. D **90**, 054014 (2014) doi:10.1103/PhysRevD.90.054014 [arXiv:1408.1627 [hep-ph]].
- [16] Y. Amhis *et al.* [Heavy Flavor Averaging Group (HFAG)], arXiv:1412.7515 [hep-ex].
- [17] A. Dedes, J. Rosiek and P. Tanedo, Phys. Rev. D **79**, 055006 (2009) [arXiv:0812.4320 [hep-ph]].
- [18] A. Crivellin, L. Hofer, J. Matias, U. Nierste, S. Pokorski and J. Rosiek, Phys. Rev. D **92**, no. 5, 054013 (2015) [arXiv:1504.07928 [hep-ph]].
- [19] M. Carpentier and S. Davidson, Eur. Phys. J. C **70**, 1071 (2010) [arXiv:1008.0280 [hep-ph]].
- [20] K. Cheung, T. Nomura and H. Okada, arXiv:1610.02322 [hep-ph].
- [21] S. Chatrchyan *et al.* [CMS Collaboration], Phys. Rev. Lett. **111**, 101804 (2013) [arXiv:1307.5025 [hep-ex]].
- [22] R. Aaij *et al.* [LHCb Collaboration], Phys. Rev. Lett. **111**, 101805 (2013) [arXiv:1307.5024 [hep-ex]].
- [23] S. Sahoo and R. Mohanta, Phys. Rev. D **91**, no. 9, 094019 (2015) [arXiv:1501.05193 [hep-ph]].
- [24] A. M. Baldini *et al.* [MEG Collaboration], arXiv:1605.05081 [hep-ex].
- [25] J. Adam *et al.* [MEG Collaboration], Phys. Rev. Lett. **110**, 201801 (2013) [arXiv:1303.0754 [hep-ex]].
- [26] Review by A. Hoecker and W.J. Marciano in PDG.
- [27] J. P. Lees *et al.* [BaBar Collaboration], Phys. Rev. D **86**, 052012 (2012) [arXiv:1207.2520 [hep-ex]].
- [28] K.A. Olive *et al.* (Particle Data Group), Chin. Phys. C, **38**, 090001 (2014) and 2015 update.
- [29] K. Cheung and O. Seto, Phys. Rev. D **69**, 113009 (2004) [hep-ph/0403003].
- [30] P. A. R. Ade *et al.* [Planck Collaboration], Astron. Astrophys. **571**, A16 (2014) [arXiv:1303.5076 [astro-ph.CO]].
- [31] C. H. Chen, T. Nomura and H. Okada, arXiv:1607.04857 [hep-ph].
- [32] See for example, M. Aaboud *et al.* [ATLAS Collaboration], New J. Phys. **18**, no. 9, 093016 (2016) [arXiv:1605.06035 [hep-ex]].
- [33] M. Kramer, T. Plehn, M. Spira and P. M. Zerwas, Phys. Rev. D **71**, 057503 (2005) [hep-ph/0411038]; T. Mandal, S. Mitra and S. Seth, Phys. Rev. D **93**, no. 3, 035018 (2016) [arXiv:1506.07369 [hep-ph]].
- [34] T. Mandal, S. Mitra and S. Seth, JHEP **07**, 028 (2015) [arXiv:1503.04689 [hep-ph]]; A. Belyaev, C. Leroy, R. Mehdiyev and A. Pukhov, JHEP **0509**, 005 (2005) [hep-ph/0502067].

- [35] K. m. Cheung, Phys. Lett. B **517**, 167 (2001) [hep-ph/0106251].
- [36] ATLAS Coll., “Further searches for squarks and gluinos in final states with jets and missing transverse momentum at $\sqrt{s} = 13$ TeV with the ATLAS detector”, ATLAS-CONF-2016-078.
- [37] M. Aaboud *et al.* [ATLAS Collaboration], Eur. Phys. J. C **76**, no. 10, 547 (2016) [arXiv:1606.08772 [hep-ex]].
- [38] I. de Medeiros Varzielas and G. Hiller, JHEP **1506**, 072 (2015) [arXiv:1503.01084 [hep-ph]]; G. Hiller, D. Loose and K. Schonwald, arXiv:1609.08895 [hep-ph]; D. Becirevic, S. Fajfer and N. Kosnik, Phys. Rev. D **92**, no. 1, 014016 (2015) [arXiv:1503.09024 [hep-ph]].